npj | parkinson's disease

Article

Published in partnership with the Parkinson's Foundation

https://doi.org/10.1038/s41531-024-00827-7

Cannabinoid regulation of angiotensin II-induced calcium signaling in striatal neurons

Check for updates

Rafael Rivas-Santisteban [1,2] ✉, Ana Muñoz [2,3], Jaume Lillo[2,4], Iu Raïch[2,4], Ana I. Rodríguez-Pérez [2,3], Gemma Navarro [2,4,5,8], José L. Labandeira-García [2,3,8] & Rafael Franco [2,6,7,8] ✉

Calcium ion (Ca^{2+}) homeostasis is crucial for neuron function and neurotransmission. This study focused on the actions mediated by the CB_1 receptor (CB_1R), the most abundant G protein-coupled receptor (GPCR) in central nervous system (CNS) neurons, over by the AT_1R, which is one of the few G protein-coupled CNS receptors able to regulate cytoplasmic Ca^{2+} levels. A functional interaction suggesting a direct association between these receptors was detected. AT_1-CB_1 receptor heteromers (AT_1CB_1Hets) were identified in HEK-293T cells by bioluminescence resonance energy transfer ($BRET^2$). Functional interactions within the AT_1-CB_1 complex and their potential relevance in Parkinson's disease (PD) were assessed. In situ proximity ligation assays (PLA) identified AT_1CB_1Hets in neurons, in which an important finding was that Ca^{2+} level increase upon AT_1R activation was reduced in the presence of cannabinoids acting on CB_1Rs. AT_1CB_1Het expression was quantified in samples from the 6-hydroxydopamine (6-OHDA) hemilesioned rat model of PD in which a lower expression of AT_1CB_1Hets was observed in striatal neurons from lesioned animals (versus non-lesioned). AT_1CB_1Het expression changed depending on both the lesion and the consequences of levodopa administration, i.e., dyskinesias versus lack of involuntary movements. A partial recovery in AT_1CB_1Het expression was detected in lesioned animals that developed levodopa-induced dyskinesias. These findings support the existence of a compensatory mechanism mediated by AT_1CB_1Hets that modulates susceptibility to levodopa-induced dyskinesias in PD. Therefore, cannabinoids may be useful in reducing calcium dyshomeostasis in dyskinesia.

Parkinson's disease (PD) is mostly caused by the death of dopaminergic neurons located in the substantia nigra that innervate the striatum. Dopamine deficiency in the striatum leads to unbalanced motor control causing the symptoms of rigidity and tremor that patients display[1]. Dopaminergic transmission is based mainly on the action of the five types of dopamine receptors identified so far, from D_1 to D_5. All of them are G protein-coupled receptors (GPCRs); activation of dopamine receptors leads to variation of adenosine 3′,5′-cyclic monophosphate (cAMP) intracellular levels. D_1 and D_5 receptors couple to heterotrimeric G_s transducers and, therefore, their activation causes increases in cAMP through the activation of protein kinase A (PKA)-dependent adenylate cyclase. Conversely, the D_2, the D_3, and the D_4 couple to heterotrimeric G_i transducers, and their activation causes decreases in cAMP levels through deactivation (inhibition) of the adenylate cyclase[2].

The link between dopamine receptor activation and the cAMP/PKA signaling pathway prompted the discovery and characterization of a

[1]Laboratory of Computational Medicine, Biostatistics Unit, Faculty of Medicine, Autonomous University of Barcelona, Campus Bellaterra, Barcelona, Spain. [2]Network Center for Biomedical Research in Neurodegenerative Diseases, CiberNed, Spanish National Health Institute Carlos iii, Madrid, Spain. [3]Cellular and Molecular Neurobiology of Parkinson's Disease, Research Center for Molecular Medicine and Chronic Diseases (CIMUS), IDIS, University of Santiago de Compostela, Santiago de Compostela, Spain. [4]Department of Biochemistry and Physiology, School of Pharmacy and Food Sciences, Universitat de Barcelona, Barcelona, Spain. [5]Institute of Neuroscience of the University of Barcelona, Universitat de Barcelona, Barcelona, Spain. [6]Molecular Neurobiology Laboratory, Dept. Biochemistry and Molecular Biomedicine, Facultat de Biologia, Universitat de Barcelona, Barcelona, Spain. [7]School of Chemistry, Universitat de Barcelona, Barcelona, Spain. [8]These authors contributed equally: Gemma Navarro, José L. Labandeira-García, Rafael Franco.
✉e-mail: rrivasbioq@gmail.com; rfranco@ub.edu; rfranco123@gmail.com

dopamine-regulated neuronal phosphoprotein, abbreviated as DARPP-32; being 32 its apparent molecular weight in kilodaltons. DARPP-32 is prone to be phosphorylated in a PKA-dependent manner and was first described as an inhibitor of protein phosphatase 1[3,4]. There are multiple actions linked to the activity of DARPP-32 in neurons of the basal ganglia both in health and disease. Apart from its role in motor control by integrating the D_1- and the D_2-receptor-mediated signaling, DARPP-32 is involved in synaptic plasticity (see ref. 5 for review).

Cannabinoids are crucial neuromodulators that act primarily through the CB_1 cannabinoid receptor (CB_1R), which is the most abundant GPCR in the CNS[6]; it is expressed in neurons but also in glial cells. Activation of CB_1R, which is coupled to G_i, inhibits dopamine action in neurons expressing G_s-coupled D_1 receptors and DARPP-32 whereas it amplifies dopamine actions in neurons expressing G_i-coupled D_2 receptors and DARPP-32. Various cannabinoids, both natural (phytocannabinoids) and synthetic, have been tested in animal models of PD with apparent benefits[7]. A recent example is VCE-003, a synthetic cannabigerol derivative, which has shown effectiveness in the 6-hydroxydopamine (6-OHDA)-based rat model of PD [8]. These translational studies (see refs. 9,10 for review) have raised hopes about the potential to increase the therapeutic arsenal to combat PD.

Neurons depend on the calcium ion (Ca^{2+}) for their proper functioning[11]. The finding of a direct link between dopamine and neuronal Ca^{2+} handling was elusive until Susan R. George's laboratory proved that interacting dopamine receptors could couple to heterotrimeric G_q transducers. Through phospholipase C, the engagement of G_q produces inositol triphosphate, which upon binding to receptors in the endoplasmic reticulum triggers the release of Ca^{2+} to the cytoplasm. Heteromers formed by D_1 and D_2 receptors do not couple to G_i or G_s but to G_q; therefore, dopamine acting on D_1/D_2 receptor heteromers leads to the increase of Ca^{2+} cytoplasmic levels[12]. This discovery was challenged due to the apparent segregation of D_1- and D_2-expressing neurons in the striatum. Doubts arising from biased tests in rodents led to the identification in the primate brain that between 15 and 20% of neurons in the striatum express both D_1 and D_2 receptors[13]. Subsequent studies demonstrated that the mechanisms mediated by dopamine action were more diverse than previously thought and that the dopamine/Ca^{2+} link was relevant to explain why dopamine is so deeply involved in reward mechanisms and to include the Ca^{2+} in the pathophysiological mechanisms underlying nigral death and parkinsonism[14–21], thus supporting previous results such as the one showing that Ca^{2+}-calmodulin kinase II dysfunction correlates with motor and synaptic deficits in experimental parkinsonism[22].

Angiotensin II (Ang II), the main renin–angiotensin system (RAS) effector, is an octapeptide produced by the successive action of the enzymes renin and angiotensin-converting enzyme that act on the precursor angiotensinogen. RAS has been extensively studied in the periphery due to its role in controlling blood pressure[23]. The CNS has a local paracrine RAS that is dysregulated in PD[24]. In addition to the expression of RAS components in the nigra and/or striatum, hyperactivation of AT_1 receptors promotes neuroinflammation, oxidative stress, and dopaminergic death[25,26]. The nigrostriatal system is now considered to be an important center of dopamine/Ang II interaction. There are two Ang II receptor types so far identified: the angiotensin II type 1 (AT_1) and the angiotensin II type 2 (AT_2). The two receptors belong to the GPCR superfamily and whereas the AT_2 receptor preferentially couples to G_i, the AT_1R may couple to G_i, but also to G_q. In a heterologous system, we have confirmed that activation of human AT_1Rs leads to the mobilization of Ca^{2+} from the endoplasmic reticulum to the cytoplasm[27]. Other important data are that (i) AT_1R is upregulated in the striatum when there is a decrease in dopaminergic function[28,29], (ii) agonistic autoantibodies for AT_1R have been detected in samples from PD patients[30] and (iii) single-cell genomic profiling of human dopaminergic neurons identified the AT_1 receptor gene as a marker of the most vulnerable dopaminergic neurons in humans[31–33].

The objective of this study was to evaluate the interrelationships established between neuromodulators relevant to striatal function, namely endocannabinoids and Ang II. The study is based in a seminal work showing that the CB_1R and the AT_1R do form heteromers that mediate the pathogenic effects of Ang II[34]. A direct association of the two receptors to form AT_1-CB_1 receptor heteromers (AT_1CB_1Hets) was confirmed by bioluminescence resonance energy transfer assays ($BRET^2$). We focused on the actions mediated by the CB_1 receptor, the most abundant GPCR in CNS neurons, and the AT_1R, which is involved in increasing cytoplasmic Ca^{2+} levels and in calcium-mediated signaling in neurons. The first relevant finding was that G_q coupling upon AT_1R activation was altered by CB_1R expression. Our results suggest that cannabinoids decrease the AT_1R-mediated calcium signaling in striatal neurons. In situ proximity ligation assays (PLA) confirmed in striatal primary neurons the expression of AT_1CB_1Hets. In addition, the expression of receptor complexes in $NeuN^+$ cells was assessed in striatal sections of control and 6-OHDA lesioned rats and of lesioned rats treated with levodopa expressing or not dyskinesias.

Results

Functionality assays in HEK-293T cells expressing cannabinoid CB_1 and/or angiotensin AT_1 receptors

The HEK-293T-cell-based heterologous system was used to express the human versions of the Ang II type 1 (AT_1R) and the cannabinoid type 1 (CB_1R) receptors. First, the G_i-mediated signaling was assayed in cells expressing AT_1Rs and/or CB_1Rs using selective agonists and/or antagonists of the two receptors and treated with forskolin (FK), which activates adenylate cyclase to increase the intracellular levels of the cyclic nucleotide. In cells expressing only one receptor, the selective antagonist of the CB_1R, rimonabant, did not affect signaling of the AT_1R (Supplementary Fig. S1A), and candesartan, the antagonist or the AT_1R, did not affect signaling of the CB_1R (Supplementary Fig. S1B). The cAMP levels determined in FK-treated cells expressing the AT_1R showed G_i coupling due to the decrease produced by the 15-min incubation with Ang II. The effect was prevented by the selective antagonist, candesartan (Fig. 1A). Analogously, the cAMP levels induced by FK in CB_1R-expressing cells were reduced by the selective agonist, arachidonoyl 2′-chloroethylamide (ACEA). Pretreatment with rimonabant, the selective CB_1R antagonist, prevented the effect of ACEA (Fig. 1B). In cells coexpressing the two receptors, the two agonists, Ang II and ACEA, were able to decrease cAMP, suggesting G_i coupling of AT_1R and CB_1R. Simultaneous treatment with the two agonists did not lead to either synergism or additive effect. However, there was a finding, the prevention by rimonabant of the action of Ang II (Fig. 1C), that cannot be explained if the receptors are not interacting (physically or functionally). This cross-antagonism, i.e., the fact that the selective antagonist of one receptor is preventing the action of the agonist of the other receptor is suggestive of direct interaction, i.e., of the formation of AT_1CB_1Hets.

The measurement of the degree of extracellular signal-regulated kinase (ERK) 1/2 phosphorylation in the presence of agonists showed that the two receptors, when expressed individually in HEK-293T cells, are linked to the mitogen-activated protein kinase (MAPK) signaling pathway. The effect was specific as it was blocked by selective antagonists (Fig. 1D, E). In cells coexpressing the two receptors, there was a bidirectional cross-antagonism, i.e., candesartan, the AT_1R antagonist, prevented the action of ACEA, the CB_1R agonist, and rimonabant, the CB_1R antagonist, prevented the action of Ang II on the AT_1R. (Fig. 1F). Again, these findings are consistent with a molecular interaction of the two receptors.

Colocalization and interaction between cannabinoid CB_1 and angiotensin AT_1 receptors

Colocalization in HEK-293T cells expressing the two receptors was assayed by immunocytochemical techniques using receptors fused to *Renilla* luciferase (Rluc) and/or yellow fluorescent protein (YFP). First, the individual expression of each receptor was checked in cells transfected with cDNA coding for AT_1R fused to YFP or with cDNA coding for CB_1R fused to YFP; the fluorescence due to YFP excitation was observed in the two conditions (Fig. 2A, B). Coexpression was achieved by transfecting with cDNAs coding for AT_1R-Rluc and CB_1R-YFP. AT_1R-Rluc was detected by a mouse monoclonal anti-Rluc antibody and a secondary sulfo-cyanine3 (Cy3)-

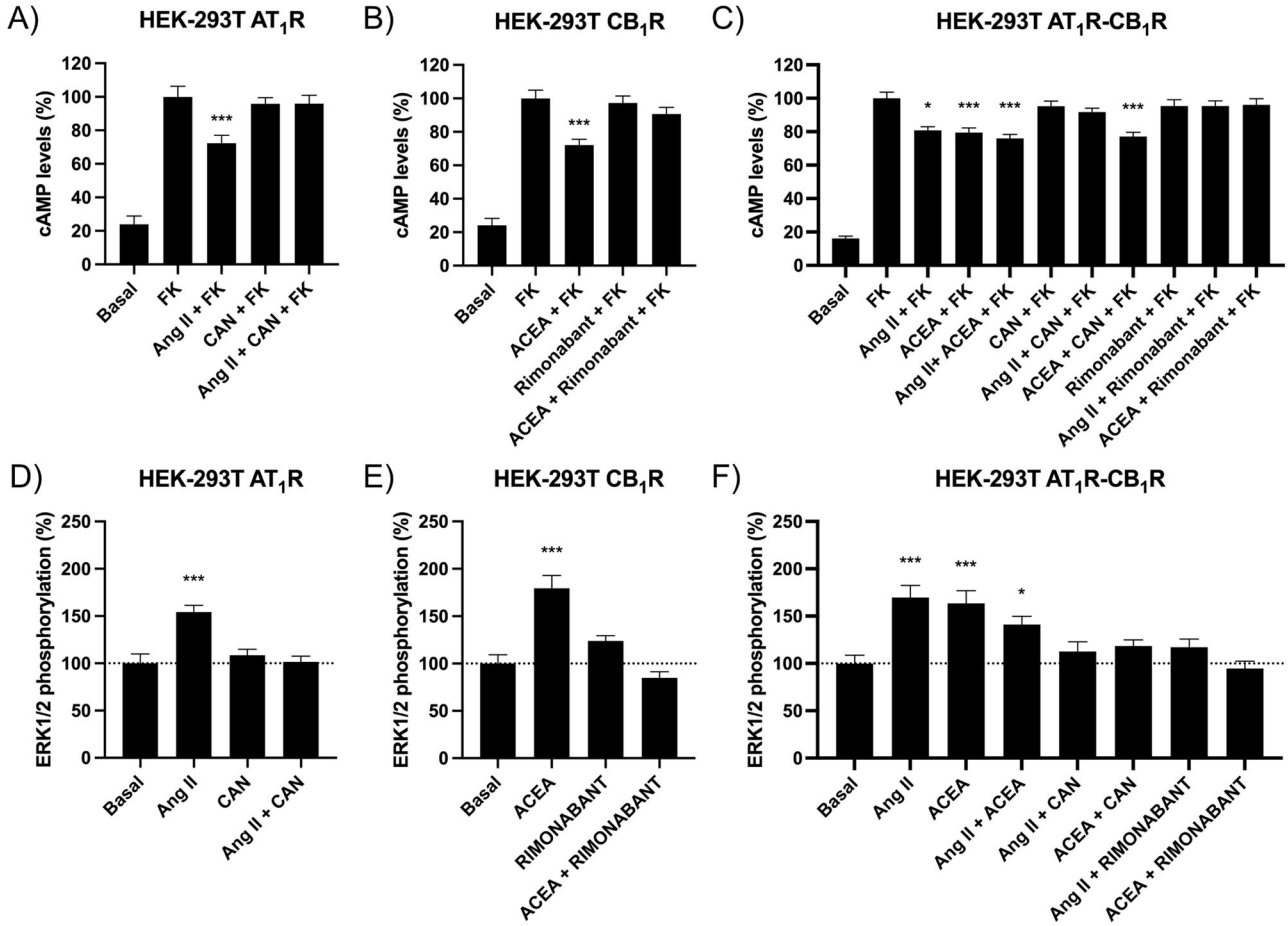

Fig. 1 | cAMP level determination and ERK1/2 phosphorylation assays in HEK-293T cells expressing AT_1 and/or CB_1 receptors. HEK-293T cells expressing, as indicated, one or both receptors were pretreated with the solvent of ligands (vehicle) or selective receptor antagonists (1 μM candesartan for AT_1R or 1 μM rimonabant for CB_1R) and subsequently treated with selective agonists (100 nM Ang II for AT_1R and/or 100 nM ACEA for CB_1R). **A**–**C** G_i protein coupling was assessed by measuring the decreases in FK-induced [cAMP] levels; 0.5 μM FK was used (added 15 min after the treatment with agonists). Values are the mean ± S.E.M. of six independent experiments performed in triplicates. Statistical analysis was performed using one-way ANOVA followed by Bonferroni's post-hoc test ($^*p < 0.05$, $^{***}p < 0.001$; versus FK condition to determine significant decreases in cAMP levels). **D**–**F** ERK1/2 phosphorylation was analyzed using an AlphaScreen®SureFire® kit (PerkinElmer). HEK-293T cells were transfected with cDNAs for AT_1R (1 μg) and/or CB_1R (1 μg). Values are the mean ± S.E.M. of three independent experiments performed in duplicates. Statistical analysis was performed using one-way ANOVA followed by Bonferroni's post-hoc test ($^*p < 0.05$, $^{***}p < 0.001$; versus basal condition to determine significant increases in ERK1/2 phosphorylation).

conjugated anti-mouse IgG antibody; CB_1R-YFP was detected by the fluorescence emitted by YFP upon excitation (see scheme in Fig. 2D). Marked overlap of the signal in the two detection channels suggested a high degree of receptor colocalization (Yellow, Fig. 2C). To check whether colocalization could result from a direct interaction between the two proteins expressed, bioluminescence resonance energy transfer 2 ($BRET^2$) assays were performed. The experiment was performed in HEK-293T cells expressing a constant amount of CB_1R-Rluc and increasing levels of AT_1R-GFP^2 (see scheme in Fig. 2G). The saturation curve shown in Fig. 2E demonstrates that the two receptors may interact in a heterologous expression system. Negative control using CB_1R-Ruc and angiotensin-converting enzyme 2 (ACE2) fused to GFP^2 led to a linear relationship between the $BRET^2$ signal and the donor/acceptor ratio, indicating no interaction (Fig. 2F).

Alteration of AT_1R-mediated G_q signaling in cells coexpressing AT_1 and CB_1 receptors

Upon discovering that AT_1 and cannabinoid CB_1 receptors interact in HEK-293T cells, we undertook assays to determine the levels of cytosolic Ca^{2+} and to test whether the receptor–receptor interaction regulates the coupling of the AT_1R to the G_q family of transducers. As noted in the "Methods" section, the experimental setup took advantage of a calmodulin-based calcium ion sensor that emits fluorescence when bound to Ca^{2+} and it is excited at the appropriate wavelength.

In cells expressing the AT_1R, but not the cannabinoid receptor, the agonist, Ang II, caused a marked increase in fluorescence, which did not decay after 150 s of measurement (Fig. 3A). The maximal effect Ang II-mediated on calcium release was completely abolished by pretreatment with candesartan, while pretreatment with rimonabant did not alter Ang II-mediated calcium mobilization (Fig. 3D). As expected, ACEA did not produce any signal in cells expressing the CB_1 receptor (Fig. 3B); the fluorescence signal was barely detectable (Fig. 3E). In cells that coexpressed the two receptors, the effect of Ang II was significant, but with different kinetics compared to the signal observed in cells that expressed only AT_1R. In fact, in cotransfected cells, Ang II led to a significant increase in fluorescence that did decay, i.e., a peak of fluorescence was observed (at around 90 s, Fig. 3C). Furthermore, ACEA, which by itself did not lead to any effect, significantly reduced the effect of Ang II also modifying the kinetics; when cells were treated with both ACEA and Ang II the peak of calcium-calmodulin sensor fluorescence was found at <50 s. Finally, while candesartan, the selective AT_1R antagonist, completely prevented the response, rimonabant, the CB_1R antagonist, reduced the Ang II response with a fluorescence peak observed around 40 s (Fig. 3C). In cells that coexpressed the two receptors, the maximal effect of Ang II-mediated on calcium release

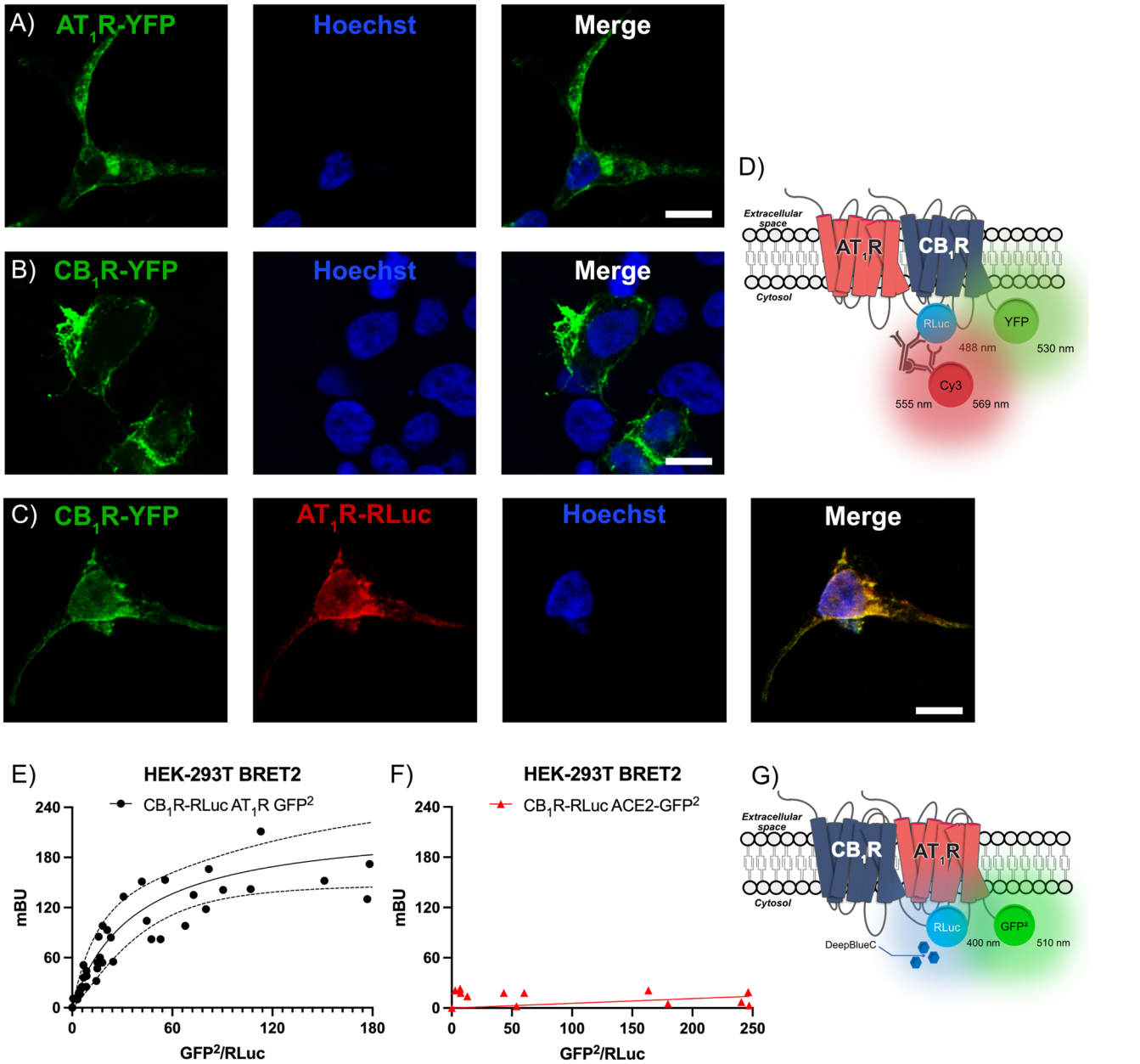

Fig. 2 | Immunocytochemistry and BRET assays. Immunocytochemistry in HEK-293T cells expressing AT_1R-YFP (**A**), CB_1R-YFP (**B**) or coexpressing AT_1R-Rluc and CB_1R-YFP (**C**). The Rluc-containing fusion protein was detected using a mouse monoclonal anti-Rluc antibody and a secondary Cy3-conjugated anti-mouse IgG antibody (red). Cell nuclei were stained with Hoechst 33342. Colocalization is shown in yellow (**C**). Confocal images were obtained at lower planes, where the plasma membrane extends on the glass of the slide. Scale bar: 15 µm. Scheme of the immunofluorescence detection (**D**). Bioluminescence resonance energy transfer $BRET^2$ assays were performed in HEK-293T cells transfected with a constant amount of cDNA for CB_1R-Rluc (0.2 µg) and increasing amounts of cDNAs for AT_1R-GFP^2 (0.5–4.5 µg) (**E**) or ACE2-GFP^2 (0.25–2 µg) (**F**, negative control). The values shown in each graph were obtained from data from six independent experiments. **G** Scheme of the $BRET^2$ assay.

was significantly reduced in both cells treated with ACEA and in cells pretreated with rimonabant (Fig. 3F). Taken together, the results indicate that CB_1R occupancy by agonists or antagonists reduces the effect of Ang II and modifies the kinetics of cytosolic Ca^{2+} release/reuptake.

Expression of AT_1CB_1Hets and functionality assays in primary striatal neurons

The in situ PLA is instrumental in detecting receptor–receptor complexes in primary cells or tissue sections. The procedure was performed as described in "Methods" section using primary striatal neurons incubated with anti-AT_1R and anti-CB_1R antibodies and, subsequently, with secondary antibodies conjugated to complementary oligonucleotide probes. AT_1-CB_1 receptor complexes (Fig. 4B) are identified by red fluorescence dots (nuclei are labeled in blue by Hoechst 33342) in structures also labeled using an Alexa-488 conjugated anti-NeuN antibody. The negative control was obtained without the anti-mouse PLA probe secondary antibody (Fig. 4A). The graph indicating the number of points per neuron (≈5.7) and the percentage of cells expressing receptor–receptor complexes (>82%) is found in Fig. 4C. Expression of AT_1CB_1Hets was also assessed in structures also labeled using an Alexa-488 conjugated anti-MAP2 antibody. The negative control was obtained without the anti-mouse PLA probe secondary antibody (Fig. 4D). Data in Fig. 4E suggest that the majority of the label is located more in the neuronal soma that in extension. On average 5.7 dots/cell were counted near $NeuN^+$ stain (Fig. 4C) while 9.3 dots/cell were counted near

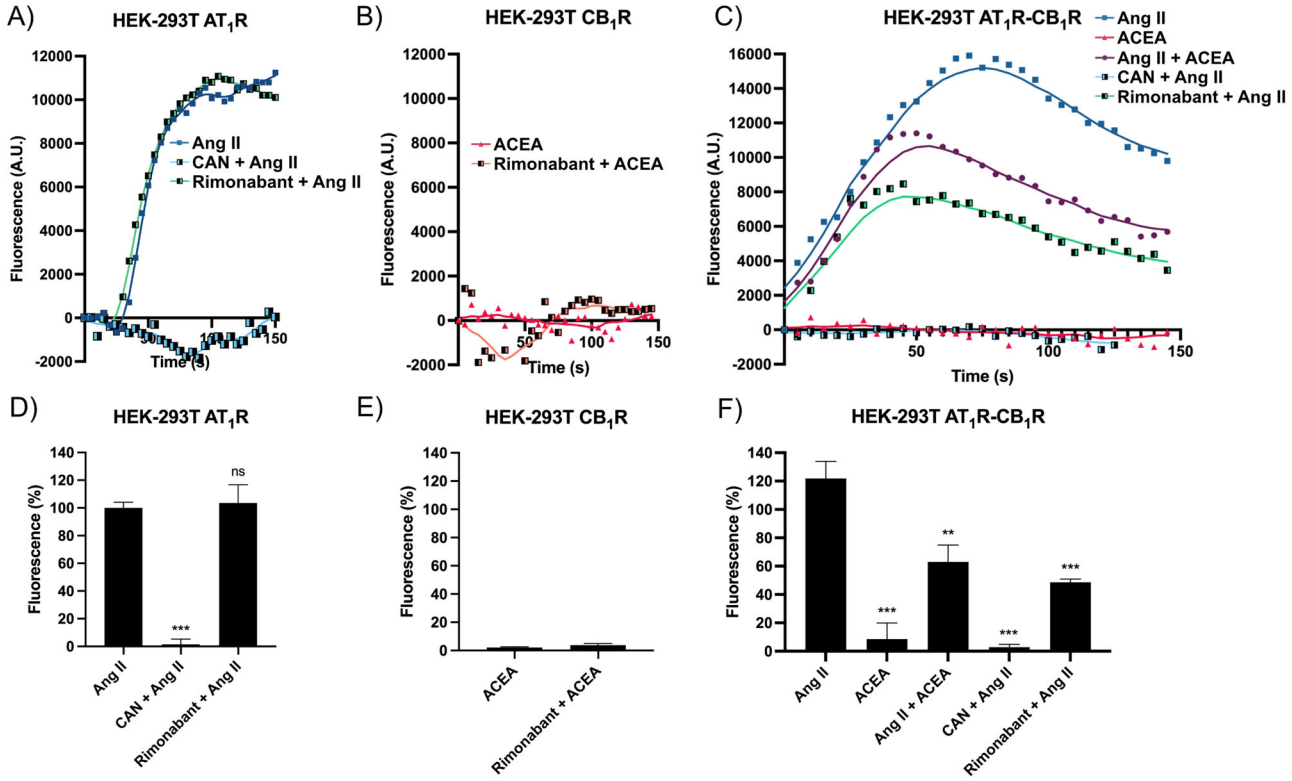

Fig. 3 | Intracellular calcium determination assays in HEK-293T cells expressing AT_1 and/or CB_1 receptors. HEK-293T cells transfected with the cDNAs for an engineered calcium sensor, 6GCaMP (1 μg), and AT_1R (1 μg) and/or CB_1R (1 μg) (**A**–**C**) were pretreated with ligand solvent (vehicle) or selective receptor antagonists (1 μM candesartan for AT_1R or 1 μM rimonabant for CB_1R) and subsequently treated with selective agonists (100 nM Ang II for AT_1R and/or 100 nM ACEA for CB_1R). Fluorescence measurements were taken every 5 s for a total time of 150 s. The fluorescence readings of a representative assay are shown in (**A**–**C**). The maximum fluorescence values for each condition have been normalized to the mean fluorescence values obtained in the Ang II condition in AT_1R-expressing cells (100%) (**D**–**F**). Values are the mean ± S.E.M. of five independent experiments performed in duplicates. Statistical analysis was performed using one-way ANOVA followed by Dunnett's post-hoc test (**D**, versus Ang II treatment ns. $p > 0.05$; ***$p < 0.001$; and **F**, versus Ang II treatment **$p < 0.01$; ***$p < 0.001$).

$MAP2^+$ structures (Fig. 4F); it may be deduced that 39% complexes are in dendrites, and 61% in neuronal somas.

Assays of determination of intracellular cAMP levels were performed in primary neurons of the rodent corpus striatum using agonists and antagonists of CB_1 and AT_1 receptors. The levels of the cyclic nucleotide induced by the treatment with FK were decreased by both, Ang II and ACEA, despite simultaneous treatment with the two agonists did not lead to a greater effect. The results obtained when neurons were pretreated with antagonists were like those found in the heterologous expression system, i.e., the antagonist of the AT_1R prevented the effect of Ang II but not the effect of ACEA, whereas the antagonist of the CB_1R prevented the effect of ACEA, but also the effect of Ang II (Fig. 4G). In ERK1/2 phosphorylation assays the results were also like those described for HEK-293T cells coexpressing the two receptors. Ang II and ACEA increased the phosphorylation levels and both the antagonists, candesartan and rimonabant, prevented the effect of each agonist. The only difference between results in primary neurons and cotransfected HEK-293T cells is that the simultaneous treatment in striatal neurons with the two receptor agonists did not result in any measurable signal (Fig. 4H). In summary, the results show that these primary neurons of the striatum express AT_1CB_1Hets and that the occupancy of the CB_1R by agonists and/or antagonists affects the signaling mediated by the AT_1R.

Cytosolic calcium levels in primary striatal neurons treated with receptor agonists

Primary striatal cultures loaded with Fluo-4 NW were treated with receptor ligands to understand whether CB_1R activation alters the AT_1R-mediated response that leads to increases in cytoplasmic Ca^{2+} concentration. Real-time measurements were performed taking images every 600 ms in a confocal microscope and the results are displayed in Fig. 5. Neurons within a given region of interest (ROI) responded to 100 nM Ang II with a rapid spike after which fluorescence slowly decreased; after 8 min of recording, the fluorescence did not return to baseline (Fig. 5A, B). The signal was completely abolished by the selective AT_1R antagonist, candesartan; in the presence of this antagonist, Ang II failed to produce a significant level of fluorescence ($\Delta F/F_0 < 0.1$, data not shown). When Ang II was administered with ACEA, the CB_1R agonist, the signal in all neurons within the ROI was much lower than that obtained in the absence of the cannabinoid (Fig. 5C, D). ACEA reduced the $\Delta F/F_0$ peak by approximately half (Fig. 5A, C) and the fluorescence reached the baseline value in <90 s (Fig. 5C). These data confirm that cannabinoid modulation of AT_1R-mediated calcium signaling occurs not only in transfected HEK-293T cells but also in striatal neurons.

Expression of AT_1CB_1Hets in the striatum of a parkinsonian rat model

The in situ PLA was used to detect receptor complexes in sections from the striatum of the 6-OHDA hemilesioned rats. Samples were collected from four animal groups: (i) control (non-lesioned), (ii) lesioned, (iii) lesioned levodopa-treated non-dyskinetic, and (iv) lesioned levodopa-treated dyskinetic. According to the tyrosine hydroxylase (TH) labeling displayed in Fig. 6A–D, the lesion was virtually complete (>95%) in the right striatum of all animal groups. The loss of dopaminergic terminals in the lesioned hemisphere is not recovered with levodopa treatment. Dyskinesia does not occur in all animals treated with levodopa and when it does occur, serotonergic pathways are likely to be involved[35,36]. The amount of AT_1R and CB_1R complexes was markedly high in striatal $NeuN^+$ neurons from non-lesioned animals and less abundant in the other animal groups (Fig. 6E–H). The label was negligible in the negative control made by omitting one of the

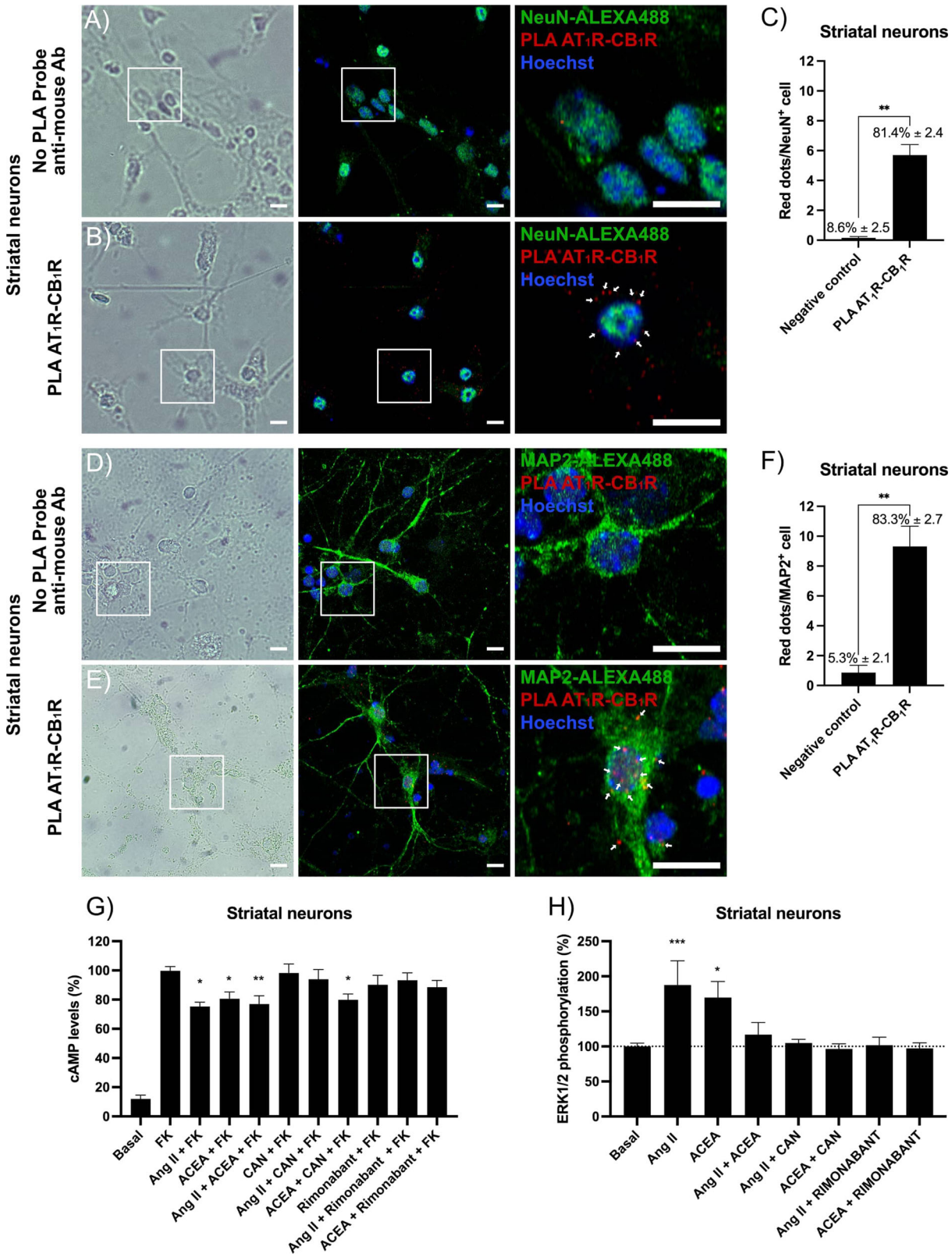

two primary antibodies (Fig. 6I). Samples from lesioned animals showed significantly fewer AT_1CB_1Hets red dots per $NeuN^+$ cell (>95% in non-lesioned versus ≈45% in lesioned). Striatal neurons expressing receptor complexes were ≈23% in levodopa-treated non-dyskinetic, and ≈70% in levodopa-treated non-dyskinetic. The number of complexes per neuron decreased in lesioned animals; interestingly, the number of complexes was further reduced in levodopa-treated non-dyskinetic animals whereas it was slightly recovered in dyskinetic animals (Fig. 6J). In summary, expression of AT_1CB_1Hets in striatal neurons varies depending on both the lesion and the consequences of levodopa treatment of lesioned rats.

Fig. 4 | AT_1R-CB_1R heteromer expression and functionality in primary striatal neurons. A–F In situ proximity ligation assays were performed in primary neurons using specific primary anti-AT_1R (1:100) and anti-CB_1R (1:100) antibodies. Cell nuclei were stained with Hoechst 33342 (blue); AT_1R-CB_1R receptor complexes appear as red dots (**B**, **E**; white arrows in the image on the right). An Alexa Fluor® 488 conjugated anti-NeuN antibody (1:200) or Alexa Fluor® 488 conjugated anti-MAP2 (1:200) were used to locate red dots in neurons. Bright-field images are shown in the left panels. Representative images corresponding to stacks of four sequential planes are shown. Scale bar: 15 µm. The number of red dots/$NeuN^+$ cells (bar graph, **C**) or red dots/$MAP2^+$ cells (bar graph, **F**) was quantified using a specifically designed pipeline of Cellprofiler™ (see "Methods" section and Supplementary Fig. S2). The percentage ± S.E.M. of neurons with at least one detected red dot out of the total number of quantified neurons is expressed above each bar. **G**, **H** Neurons were pretreated for 15 min with ligand solvent (vehicle) or selective antagonists: candesartan for the AT_1R or rimonabant for the CB_1R. Cells were then treated for 15 min with Ang II, ACEA or both. For cAMP level determinations assays (**G**), cells were treated for an additional 15 min with FK (0.5 µM). Values are expressed as the percentage of cAMP accumulation induced by FK. Statistical analysis was performed using one-way ANOVA followed by Bonferroni's post-hoc test ($^*p < 0.05$, $^{**}p < 0.01$; versus FK condition to determine significant decreases in cAMP levels). ERK1/2 phosphorylation determination assays were performed as described in "Methods" section; values were normalized by considering 100% the phosphorylation level obtained in the absence of agonists (basal) (**H**). Values are the mean ± S.E.M. of five different experiments performed in triplicates. Statistical analysis was performed using one-way ANOVA followed by Bonferroni's post-hoc test ($^*p < 0.05$, $^{***}p < 0.001$; versus basal condition to determine significant increases in ERK1/2 phosphorylation).

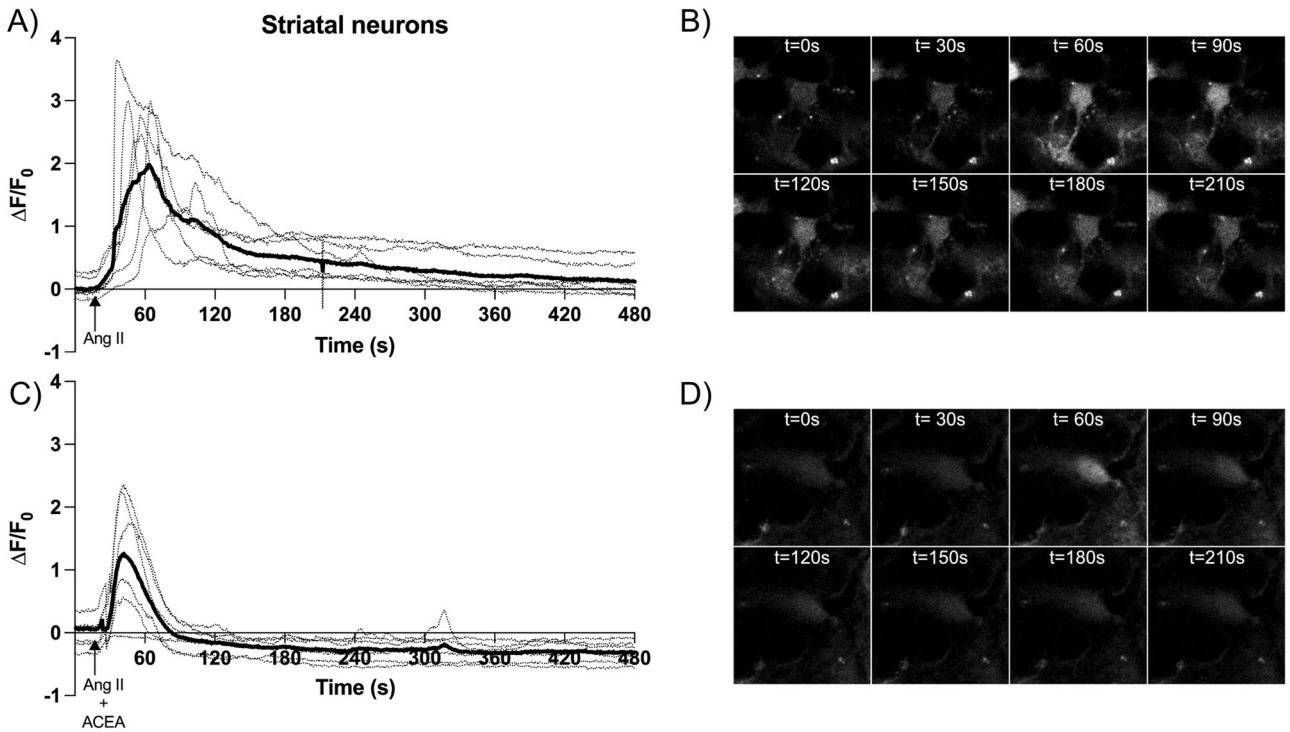

Fig. 5 | Measurement of cytosolic [Ca^{2+}] in striatal neurons loaded with Fluo-4 NW. Baseline fluorescence (F_0) was established with 15-s frames taken before adding the receptor ligands: 100 nM Ang II (**A**) or 100 nM Ang II plus 100 nM ACEA (**C**). Frames were captured at the maximum allowed speed (600 ms) by a Zeiss LSM 880 confocal microscope. Each $\Delta F/F_0$ versus time dashed curve in (**A**) and (**C**) corresponds to a single neuron; the solid black $\Delta F/F_0$ versus time curves in (**A**) and (**C**) result from averaging the readings of all neurons labeled within the ROI. Background fluorescence (F_B) was estimated by measuring fluorescence in "empty" spaces. Time series fluorescence images in (**B**) and (**D**) correspond to those qualitatively displayed in, respectively, (**A**) and (**C**). Data from a representative experiment are shown.

Discussion

Cannabinoids are neuromodulators that act mainly through CB_1 and CB_2 receptors, which can be expressed in both neurons and glia. Over decades drug development programs have focused on phytocannabinoids and synthetic cannabinoids as potential tools to combat neurodegenerative diseases. A recent example is VCE-003.2, a synthetic cannabigerol derivative, which has been shown to have benefits in the rodent model of PD induced by 6-OHDA lesion[8]. More importantly, molecules that act on cannabinoid receptors may be neuroprotective, that is, they have the potential to slow the progression of Parkinson's, Alzheimer's, and other neurodegenerative diseases[10,37–46]. Despite accumulating evidence of efficacy in neuroprotection, the exact mechanism by which cannabinoids prevent or delay neuronal death remains elusive.

Proper calcium ion handling/homeostasis is crucial in neuronal functioning in both health and disease. Disbalances in Ca^{2+} currents and Ca^{2+}-mediated signal transduction correlate with neurodegeneration. The results of this study show that cannabinoids are not only able to modulate the level of cAMP via G_i-coupling to CB_1Rs but also to regulate Ca^{2+} signaling via the establishment of receptor–receptor interactions with the AT_1R. AT_1Rs are among the few GPCRs in nigral and striatal neurons that, upon activation, lead to the release of Ca^{2+} from the endoplasmic reticulum to the cytoplasm. Through AT_1CB_1Hets, endocannabinoids and Ang II cooperate in the regulation of neurotransmission and neuronal fate and ultimately mediate the neuroprotective effects of cannabinoids. Ca^{2+} binding to calmodulin participates in dopaminergic neurotransmission by physical and functional coupling to dopamine receptors[47,48] and deficiencies in calmodulin kinase II activity are associated with motor impairment and synaptic deficit in experimental PD models[22]. A recent review details the interplay between α-synuclein, ion channels, calmodulin, and calmodulin-binding proteins in the calcium dyshomeostasis occurring in PD[49].

It is conceptually relevant to consider that dopamine replacement therapy in PD targets dopamine receptors that are forming heteromers[50–52].

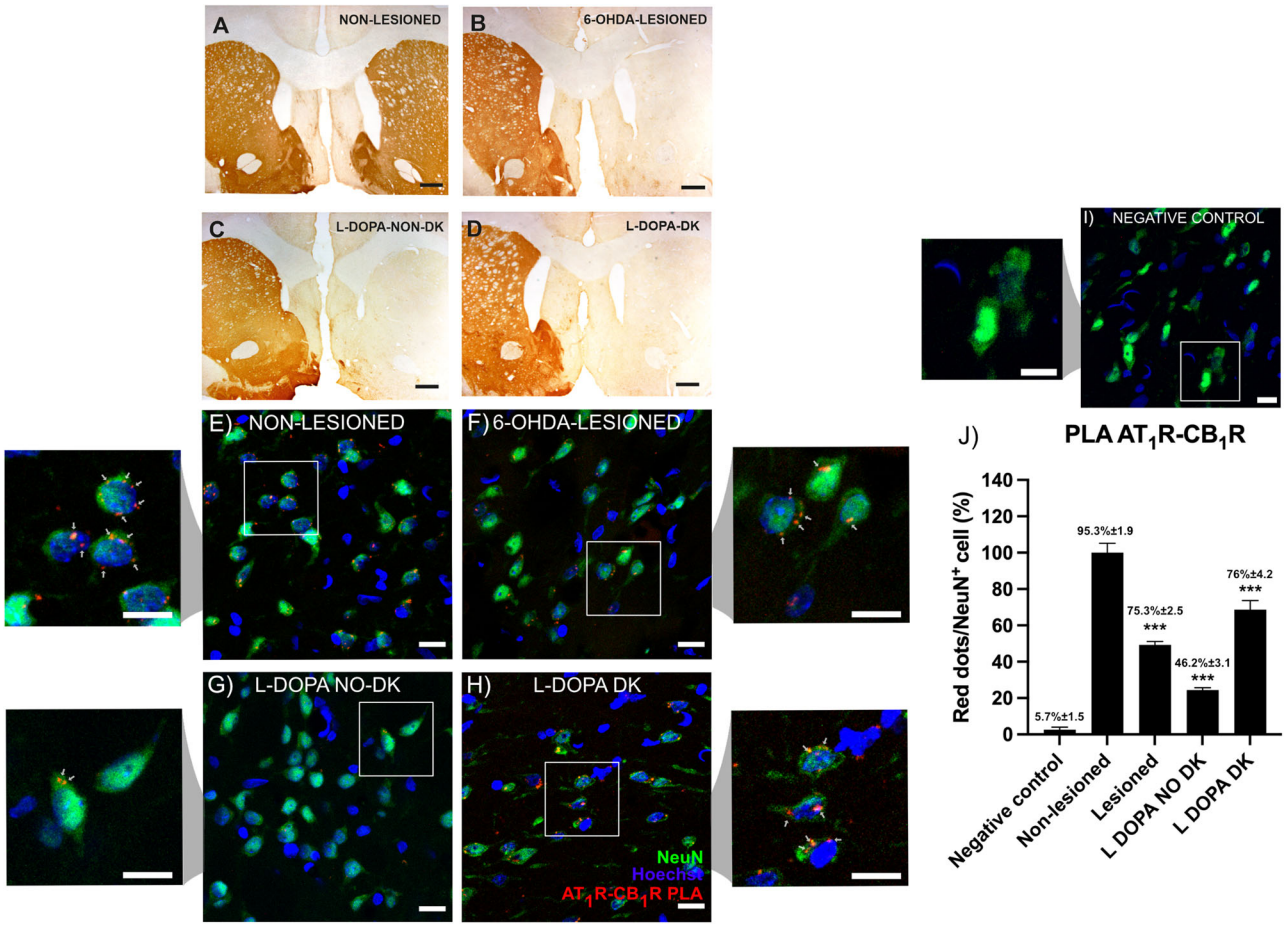

Fig. 6 | AT_1CB_1Het expression in $NeuN^+$ cells of striatal sections of control and lesioned rats. Tyrosine hydroxylase (TH) immunoreactivity in the striatum of (i) a control animal (**A**, non-lesioned), (ii) an animal with unilateral dopaminergic denervation in the right side (**B**, 6-OHDA lesioned), (iii) a lesioned animal treated with levodopa non becoming dyskinetic (**C**, L-DOPA-NON-DK) and (iv) a lesioned animal becoming dyskinetic upon levodopa treatment (**D**, L-DOPA-DK); images show a >95% -maximal- lesion in all animal groups (see "Methods" section for details). Scale bar = 500 µm. PLA assays were performed in samples from all groups. Confocal microscopy images (stacks of five consecutive planes) show AT_1CB_1Het complexes in all samples analyzed; they appear as PLA signals (red fluorescence dots) surrounding Hoechst-stained nuclei (blue). To determine whether the red dots were in neurons, Alexa-488-conjugated anti-NeuN antibodies were used (**E**–**H**). Images of the negative control, samples in which one of the oligonucleotide probes was omitted, are shown in (**I**) Scale bar = 20 µm. Bar graphs showing the percentage of red dots/$NeuN^+$ cell are in (**J**). Data are normalized by considering AT_1CB_1Hets expression in non-lesioned rats (100% refers to the number of AT_1CB_1Het per $NeuN^+$ cell in samples from non-lesioned animals). One-way ANOVA and Bonferroni's post-hoc were used to compare the red dots/cell values (***$p < 0.001$, versus non-lesioned condition). The percentage of $NeuN^+$ cells displaying at least one red dot ± S.E.M. is presented above each bar graph.

In this sense, it is worth noting that AT_1R establishes complexes with the main dopamine receptor in the so-called "indirect pathway", D_2, which, like CB_1R, couples to G_i[53]. Knowing that the RAS regulates dopaminergic neurotransmission[54], it would be worth investigating whether dopamine itself modulates responses to Ang II through G_q-coupled AT_1Rs. A previous study using a rodent neuroblastoma cell line, Neuro-2A, reported the interaction between CB_1 and AT_1 receptors and the consequences of heteromerization in terms of cAMP production and activation of the MAPK pathway[34]. Here we confirm AT_1CB_1Hets expression in a heterologous expression system, in primary striatal neurons and in striatal sections of rat brains. This specific heteromer identified in the basal ganglia complements previous results that show the relevance of cannabinoid receptor-containing heteromers for striatal function[55]. In the previous study and in the present report, a similar fingerprint of AT_1CB_1Het was found, which consists of the blockade of AT_1R-mediated signaling by the CB_1R antagonist[34]. In addition, we have identified that a highly selective synthetic CB_1R agonist decreases Ang II-mediated calcium mobilization in primary striatal neurons and in transfected HEK-293T cells. This result contrasts with the apparent synergy reported in Neuro-2A cells treated with CB_1R and AT_1R agonists[34]. The discrepancy may be due to the differential signaling pathways in a tumor-derived cell lines versus primary striatal neurons.

Our results confirm that the development of drugs targeting the CB_1R to combat PD must consider the CB_1R-containing heteromers and whether they are up or downregulated at different stages of the disease, prodromal, symptomatic, and in therapy. Furthermore, heteromer formation conditions functional selectivity, in terms of, among others, biased agonism, agonist affinity/potency and antagonist affinity[56–60].

Polymerase chain reaction and in situ assays using samples from macaque PD models show that the expression of the CB_1R in pallidothalamic-projecting neurons varies with the course of the disease[61]. In addition, treatment of PD rodent or monkey models with levodopa disrupts molecular and functional interactions of the CB_1R with the adenosine A_{2A} receptor, which is heavily expressed in the striatum, mainly in neurons of the indirect pathway, i.e., those expressing the dopamine D_2 type receptor[62,63]. We here show that whereas the lesion led to a decrease in the expression of heteromer in striatal neurons and levodopa further reduced the expression in rats that did not become dyskinetic, the level of expression was recovered in rats rendered dyskinetic upon levodopa treatment. Dyskinetic rats showed AT_1CB_1Het expression intermediate between that of lesioned and non-lesioned rats. Similar experiments performed in striatal samples from the MPTP monkey PD model showed an increase in the expression of heteromers formed by CB_1Rs and an orphan receptor that is regulated by

cannabinoids, GPR55; interestingly the expression of CB_1-GPR55 receptor heteromers in animals rendered dyskinetic by levodopa administration decreased and was similar to that of non-lesioned animals[64,65]. Taken together, the expression of CB_1R-containing heteromers can vary markedly depending on both the lesion and the animal's response to anti-symptomatic PD therapy. It appears that further reduction of AT_1CB_1Hets expression makes animals more resistant to the development of levodopa-induced dyskinesias. This counterintuitive finding, i.e., AT_1CB_1Het expression complex expression closer to that in control animals when animals became dyskinetic suggests a mechanism of compensation that involves changes in the expression of AT_1CB_1Hets. This is consistent with previous studies showing, in the same experimental model here used, that inhibition of AT_1R function using AT_1R antagonists reduces dyskinetic behavior[66]. Those findings also suggest that cannabinoids (even those lacking psychotropic effects) may be useful in combating PD-associated dyskinesia.

While quantification of AT_1-CB_1Hets in non-neuronal cells is beyond the current scope of this manuscript, it would be relevant to know it they are expressed in astrocytes, both in non-lesioned and in lesioned animals. Astrocytes play a critical role in PD pathophysiology. Dysfunctional astrocytes contribute to neuroinflammation, oxidative stress, and impaired synaptic function, exacerbating dopaminergic neuron degeneration. Glial cells are responsible for maintaining neuronal homeostasis, detoxifying reactive oxygen species, and clearing extracellular α-synuclein, a key protein involved in PD[67]. α-synuclein aggregation causes astrogliosis and activation of oligodendrocytes and of microglia[68]. Future studies would be essential to explore the functional roles of AT_1-CB_1Hets in glial cells, assessing their involvement in calcium handling could provide crucial information to advance our understanding of the mechanisms of neurodegeneration in PD.

Finally, it should be noted that AT_1 and CB_1 receptors have been reported to be expressed in the membranes of the mitochondria[69,70]. More and more data are appearing on the relevant role of mitochondria in the pathophysiology of neurodegenerative diseases[71–77]. Future work may lead to discovering AT_1CB_1Hets in the mitochondria of nigral and striatal neurons and, if so, provide insights into their role in mitochondrial alterations observed in neurons fated to die in PD.

Methods

Reagents

Forskolin (FK), Arachidonoyl 2′-chloroethylamide (ACEA), angiotensin II (Ang II), Candesartan, Rimonabant (SR141716), PolyEthylenImine (PEI), 6-hydroxy dopamine (6-OHDA), and Hoechst 33342 were purchased from Merck (St Louis, MO, USA). Concentrated (10 mM) stock solutions of agonists/antagonists prepared in ethanol (ACEA), DMSO (Candesartan and Rimonabant) or water (Ang II) were stored at −20 °C; they were thawed and diluted before use.

Cell culture and transfection

HEK-293T cells, batch 70022180, were acquired from the American Type Culture Collection (ATCC). Cells were amplified and frozen in liquid nitrogen in several aliquots. Cells from each aliquot were used until passage 18. HEK-293T cells were grown in Dulbecco's modified Eagle's medium (DMEM) (Gibco, Paisley, Scotland, UK) supplemented with 2 mM L-glutamine, 100 µg/mL sodium pyruvate, 100 U/mL penicillin/streptomycin, MEM non-essential amino acids solution (1/100) and 5% (v/v) heat-inactivated fetal bovine serum (all supplements were from Invitrogen, Paisley, Scotland, UK) and maintained at 37 °C in a humid atmosphere of 5% CO_2.

Primary striatal neurons were obtained from 19-day mouse embryos as described in refs. 78,79. Briefly, striata were dissected and digested in 0.25% trypsin for 15 min at 37 °C. Trypsinization was stopped by repeated washes with Hank's Buffered Saline Solution (HBSS, Gibco). Cells were brought to a single-cell suspension by repeated pipetting followed by passage through a 100 µm-pore mesh. Cells were then resuspended in supplemented DMEM and seeded at a density of 3.5×10^5 cells/mL in 6-well plates or 96-well plates for functional assays and in 12-well plates for immunocytochemistry or PLA assays. The day after, the medium was replaced by neurobasal medium supplemented with 2 mM L-glutamine, 100 U/mL penicillin/streptomycin, and 2% (v/v) B27 (Gibco) and cells were cultured for 12 days. Cultures were maintained at 37 °C in a 5% CO_2 humid atmosphere. Immunodetection of the NeuN marker showed that preparations contained >95% neurons.

Cell transfection

HEK-293T cells were transiently transfected with the corresponding cDNA(s) by the PEI method. Briefly, cDNA diluted in 150 mM NaCl was mixed (10 min) with PEI (5.5 mM in nitrogen residues) and prepared in 150 mM NaCl for 10 min. The cDNA–PEI complexes were placed in contact with HEK-293T cells and were incubated for 4 h in a serum-free medium. Then, the medium was replaced by a fresh supplemented culture medium and cells were maintained at 37 °C in a 5% CO_2 humid atmosphere. Forty-eight hours after transfection, cells were washed, detached, and resuspended in assay buffer/medium for further analysis.

Expression vectors

pcDNA3.1-based plasmids encoding for CB_1R, CB_1R-Rluc, CB_1R-YFP, AT_1R, AT_1R-Rluc, AT_1R-YFP, AT_1R-GFP^2 and ACE2-GFP^2 fusion proteins were used. Plasmids encoding fusion proteins were generated by subcloning the coding region of each receptor to be in-frame with restriction sites of pRluc-N1 (Clontech, Heidelberg, Germany), pEYFP-N1 (PerkinElmer, Waltham, MA, USA) and pEGFP^2-N1 (Clontech) vectors to provide plasmids that express the receptors with Rluc, YFP or GFP^2 proteins fused on the C-terminal end.

6-OHDA lesion and behavior assessment

Protocols adhered to EU directives (2010/63/EU and 86/609/CEE) and were approved by the ad hoc ethical committee. Male Wistar rats were used and the experimental procedures were similar to those elsewhere described[66,80,81]. Lesioning protocol was performed in 8-week-old rats.

Animals were anesthetized with 1% ketamine (75 mg/kg) and 2% xylazine (10 mg/kg). Twelve micrograms of 6-OHDA in 4 µL of saline containing 0.2% ascorbic acid was injected in the right medial forebrain bundle. Rotational behavior was used to confirm the lesion. Non-lesioned animals were subjected to a similar procedure but using saline instead of the neurotoxin.

A bank of 8 automated rotometer bowls (Rota-count 8, Columbus Instruments, Columbus, OH, USA) was used to monitor full (360°) body turns in either direction (90 min after i.p. injection of 2.5 mg/kg dextroamphetamine dissolved in saline). Six full body turns/min ipsilateral to the lesion corresponds to >90% depletion of dopamine fibers in the striatum[82]; however dopaminergic lesions were confirmed with the cylinder test, i.e., by analyzing spontaneous use of the forelimb[83]. A glass cylinder (20 cm in diameter) was used and the number of right or left forepaw contacts was blindly assessed. Scoring left (impaired) touches as a percentage of total touches, control animals would receive a 50% unbiased score, whereas lesioned animals that were selected for further experimentation showed <20% scores.

Levodopa-induced dyskinesia

Sixteen lesioned animals were chronically treated for 3 weeks with levodopa methyl ester (6 mg/kg) and benserazide (10 mg/kg), the administration route was subcutaneous. The treatment reliably induces dyskinetic movements in some rats. Abnormal involuntary movements that appeared in some of the treated animals were assessed by the elsewhere described dyskinesia scale[84]. The severity of each limb, orolingual, and axial involuntary movements was assessed using scores from 0 to 4 (4 = continuous, 3 = continuous but interrupted by strong sensory stimuli; 2 = frequent, present >50% of the time, and 1 = occasional, present <50% of the time. Dyskinetic rats were considered when animals displayed a score ≥2 per monitoring period on at least two types of abnormal involuntary movements). Non-dyskinetic rats exhibited no levodopa-induced abnormal

involuntary movements or mild/occasional ones. Animals with low scores, either dyskinetic or non-dyskinetic were excluded. In summary, four groups of animals were analyzed: (i) non-lesioned, (ii) lesioned, treated with vehicle; (iii) lesioned and dyskinetic and (iv) lesioned and non-dyskinetic despite levodopa treatment. TH immunostaining was performed in sections taken postmortem; lesioned animals showed >95% nigral dopaminergic denervation. PLA were performed in different fields of striatal sections. Images were captured in delimitation areas; the striatum was delimited using a bright field.

cAMP determination

Determination of intracellular 3′,5′-monophosphate (cAMP) levels was performed in primary neurons or HEK-293T cells transfected with the cDNA for AT_1R (1.5 μg), the cDNA for the CB_1R (1.5 μg) or both. The intracellular concentration of this first messenger was determined using the Lance Ultra cAMP kit (PerkinElmer). The method consists of a time-resolved fluorescence resonance energy transfer (TR-FRET) immunoassay in which endogenous cAMP competes with europium (Eu) chelate-labeled cAMP tracer for binding sites on a cAMP-specific antibody labeled with the ULightTM dye. Light pulses at 320 nm excite the Eu of the tracer. The energy emitted by the excited Eu is transferred by FRET to ULight molecules on the antibodies, which in turn emit light at 665 nm. In the absence of cAMP, maximal TR-FRET signal is achieved; when an agonist leads to an increase in cytosolic cAMP levels the competition between the unlabeled and the Eu-labeled cAMP species leads to a decrease in the TR-FRET signal, the emission fluorescence remains unmodified when equilibrium is achieved. cAMP concentrations per cell or mg protein were determined using a standard curve using pure unlabeled cAMP. Residual energy from the Eu chelate will produce light at 615 nm. The dynamic range covers from 10^{-10} to 10^{-8} M cAMP concentrations.

Neurons or transfected cells were grown in 6-well plates. Forty-eight hours post-transfection, the medium was replaced by serum-free medium (DMEM). Two hours later cells were detached, isolated by centrifugation (5 min at 1500 rpm) and resuspended in ^{cAMP}medium, which consisted of DMEM containing HEPES (5 mM, pH 7.4), zardaverine (50 μM), a phosphodiesterase inhibitor to prevent degradation of cAMP, and 0.1% bovine serum albumin (BSA). Determination was performed in 384-well plates (PerkinElmer) using 4000 cells/well.

Cells were incubated for 15 min with 2 μL of ^{cAMP}medium (to determine the basal levels of cAMP) or with 2 μL of ligands prepared in ^{cAMP}medium. When indicated antagonists (1 μM candesartan or 1 μM rimonabant) were added to cells for 15 min before addition of agonists. Fifteen minutes after addition of agonists, cells were treated for 15 min with 500 nM FK. cAMP-Europium (cAMP-Eu) (5 μL) and fluorophore-containing ULight™ antibody (5 μL) were then added. Incubation was prolonged for 1 h at 25 °C and the PHERAstar Flagship reader equipped with an HTRF optical module (BMG Lab Technologies, Offenburg, Germany) was used for measuring the 665/620 nm ratio.

ERK1/2 phosphorylation assay

The link to the MAPK signaling pathway was assessed by a homogeneous method, which avoids immunoblotting and directly measures levels of phosphorylated proteins in a cell-based format (AlphaScreen® SureFire® kit; PerkinElmer). The kit contains an antibody that is specific for a phospho-epitope and another that is specific for another region (distal to the phospho-epitope) of extracellular signal-regulated kinase 1 and 2 (ERK1/2). One of the antibodies is biotinylated and binds to streptavidin-conjugated donor beads, and the second binds to protein A Sepharose beads that contain an acceptor. Only immuno-complexes that contain both antibodies can bind both beads and, therefore, donor-to-acceptor energy transfer can occur. Emission fluorescence is measured using an EnSpire Multimode Plate Reader (PerkinElmer). The kit uses the AlphaScreen® technology that is based on the emission of singlet oxygen by the donor beads (which contain phthalo cyanine, excited by the red light at 680 nm), which can diffuse to reach the acceptor beads where the energy of singlet oxygen is used by a cascade (thioxene–anthracene–rubrene), leading to the emission of light at a shorter wavelength (520–620 nm range) than the excitation light. Transparent Biocat Poly-D Lysine 96-well plates (Deltalab) were used for cell culture. The assay was performed either in neurons or in transfected HEK-293T cells.

Complete medium was replaced by serum-free medium, and cells were treated or not for 10 min with the antagonists, candesartan or rimonabant followed by 7-min treatment with the selective agonists Ang II and/or ACEA. Cells were then washed twice with cold PBS before the addition of lysis buffer (15 min at 25 °C, 30 μL/well; PerkinElmer) and then incubated under agitation in a Polymax 2040 (Heidolph Instruments, Schwabach, Germany). Ten microliters of each cell lysate were transferred to 384-well microplates (white ProxiPlate; PerkinElmer). Five microliters per well of beads containing the acceptor were added and allowed to incubate in the dark for 2 h at 25 °C. Finally, 5 μL/well of beads containing the donor were added and plates were protected from the light. After 2 h incubation fluorescence was determined. The effect of ligands was given in percentage respect to the reference value (basal). The value achieved in the absence of any treatment (30 μL DMEM) was taken as a reference (basal = 100).

Immunocytochemistry

HEK-293T cells were seeded on glass coverslips in 12-well plates. Twenty-four hours after, cells were transfected with AT_1R-YFP cDNA (1 μg), CB_1R-YFP cDNA (1 μg), and/or AT_1R-Rluc (1 μg). Forty-eight hours after, cells were fixed in 4% paraformaldehyde for 15 min and washed twice with PBS containing 20 mM glycine before permeabilization with PBS-glycine containing 0.2% Triton X-100 (5 min incubation). Cells were blocked during 1 h with PBS containing 1% BSA. HEK-293T cells were labeled with a mouse anti-Rluc antibody (1/100; Millipore, Darmstadt, Germany) and subsequently treated with Cy3-conjugated anti-mouse (1/200; Jack- son ImmunoResearch (red)) antibody (1 h each). The AT_1R-YFP and CB_1R expression was detected by the YFP's own fluorescence. Nuclei were stained with Hoechst 33342 (1/100 from stock 1 mg/mL; Sigma-Aldrich). Samples were washed several times and mounted with Immu-Mount™ (ref. 9990402). Images were obtained in a Zeiss LSM 880 confocal microscope (ZEISS, Germany) with the 63× oil objectives.

Bioluminescence resonance energy transfer ($BRET^2$) assay

HEK-293T cells were transiently cotransfected with a constant amount of cDNA encoding for CB_1R-Rluc (0.2 μg) and with increasing amounts of cDNA corresponding to either AT_1R-GFP^2 (0.5–4.5 μg) or with ACE2-GFP^2 (0.25–2 μg), as a negative control for $BRET^2$ assay. To assess cell amount, protein concentration was determined using a Bradford assay kit (Bio-Rad, Munich, Germany) using BSA dilutions as standards. To quantify protein-GFP^2 expression, fluorescence was read in a Mithras LB 940 equipped with a high-energy xenon flash lamp, using a bandwidth excitation filter at 395 nm. For BRET measurements, the equivalent of 20 μg protein cell suspension was distributed in 96-well microplates (white plates, Porvair, Leatherhead, UK) and DeepBlueC (5 μM) was added (PJK GMBH, Kleinblittersdorf, Germany). Thirty seconds after DeepBlueC addition, the readings were collected using a Mithras LB 940 (Berthold, Bad Wildbad, Germany), which allowed the integration of the signals detected in the short-wavelength filter at 395 nm and the long-wavelength filter at 515 nm. To quantify receptor-Rluc expression, luminescence readings were collected 10 min after the addition of DeepBlueC (5 μM) (Molecular Probes, Eugene, OR) using a Mithras LB 940.

Determination of cytoplasmic calcium ion (Ca^{2+}) levels

HEK-293T transfected with the cDNAs for AT_1R and/or CB_1R were also transfected with the cDNA for the GCaMP6 calcium sensor (1 μg)[85]. Forty-eight hours post-transfection, HEK-293T cells were detached using Mg^{2+}-free Locke's buffer (154 mM NaCl, 5.6 mM KCl, 3.6 mM $NaHCO_3$, 2.3 mM $CaCl_2$, 5.6 mM glucose, 5 mM HEPES, 10 μM glycine, pH 7.4), centrifuged for 5 min at 3200 rpm and resuspended in the same buffer. Protein concentration was quantified by using the Bradford assay kit (Bio-Rad, Munich,

Germany). To measure Ca^{2+} mobilization, cells (40 µg of protein) were distributed in 96-well microplates (black plates with a transparent bottom; Porvair, Leatherhead, UK) and were preincubated for 10 min with antagonists, when indicated, before adding AT_1R agonist (Ang II, 100 nM) and/or CB_1R agonist (ACEA, 100 nM) right before readings. Fluorescence emission intensity due to GCaMP6 was recorded at 515 nm upon excitation at 488 nm on the EnSpire® Multimode Plate Reader for 150 s every 5 s at 100 flashes per well.

For real-time detection of cytoplasmic calcium ion (Ca^{2+}) levels in striatal neurons, cells were seeded in Lab-Tek® Chambered #1.0 Borosilicate cover glass devices (ref. 155411, ThermoFisher), coated with poly-D-lysine (ref. 16021412, Gibco), and then incubated for 15 days. After this period, neurons were washed three times with HBSS. Then, neurons were incubated with the Fluo-4 NW Ca^{2+} indicator (ref. 10266762, Fisher Scientific) for 1 h at 37 °C. Eight-well chambers were then observed under a Zeiss 880 confocal microscope (Carl Zeiss, Oberkochen, Germany) with the 40× oil immersion objective. The excitation wavelength was 488 nm, and the emission wavelength was 516 nm. To establish baseline fluorescence (F_0) images were taken for 15 s before adding ligands. Next, the AT_1R agonist (Ang II, 100 nM) and/or the CB_1R agonist (ACEA, 100 nM) were added, and images were captured at the maximum allowed speed (600 ms) for a total period of 8 min. Background fluorescence (F_B) was estimated by measuring fluorescence in cell-free spaces. The auto-focus option was activated in each observation to avoid blurring after applying the treatment. $\Delta F/F_0$ ratio was used for quantification. This normalization helps to report variations in the initial fluorescence intensity across different conditions, allowing for a more accurate comparison of the relative changes in fluorescence.

Immunohistochemistry

TH immunohistochemistry analysis was used to verify the extent of the lesion. The sections were incubated for 1 h in 10% normal swine serum with 0.25% Triton X-100 in 20 mM potassium phosphate-buffered saline, containing 1% bovine serum albumin (KPBS-BSA), and afterward incubated overnight (at 4 °C) with anti-TH as the dopaminergic marker (mouse monoclonal anti-TH, Sigma-Aldrich Cat# T2928, RRID: AB_477569; 1:10,000). Sections were then incubated with the corresponding biotinylated secondary antibody (horse anti-mouse, Vector Laboratories, Inc., Newark, CA, USA; Cat# BA-2001, RRID: AB_2336180; 1:200) for 60 min, and subsequently with an avidin–biotin–peroxidase complex (ABC, 1:100, Vector) for 90 min. Finally, sections were revealed with 0.04% hydrogen peroxide and 0.05% 3-3′diaminobenzidine (DAB, D5637, Sigma-Aldrich). Control sections in which the primary antibody was omitted were immune-negative for TH.

Proximity ligation assay (PLA)

The interaction between AT_1 and CB_1 receptors in striatal neurons and brain sections was detected using the Duolink in situ PLA detection Kit (OLink; Bioscience, Uppsala, Sweden ref. DUO92008) following the instructions of the supplier. Primary neurons grown on glass coverslips were fixed in paraformaldehyde (4%) for 15 min, washed with PBS containing glycine (20 mM) to quench the aldehyde groups and permeabilized with the same buffer containing Triton X-100 (0.05%, 20 min for primary neurons and 30 min for brain sections) and successively washed with PBS. Then, samples were incubated (1 h) at 37 °C with a blocking solution (ref. DUO82007, Sigma-Aldrich) in a pre-heated humidity chamber. After overnight incubation with the antibody diluent medium having a mixture of equal amounts of rabbit anti-AT_1R (ab124734, Abcam) (1/100) and mouse anti-CB_1R (sc-518,035, Santa Cruz) antibodies (1/100), ligation and amplification were conducted as indicated by the supplier. Neurons were identified by staining with the Alexa Fluor®488 conjugated anti-NeuN antibody (ab190195, 1/200) or Alexa Fluor®488 conjugated anti-MAP2 antibody (MAB3418X, 1/200). Samples were mounted using the mounting medium with Hoechst 33342 (1/100) to stain nuclei. Samples were observed in a Zeiss 880 confocal microscope (Carl Zeiss, Oberkochen, Germany) equipped with an apochromatic 63× oil immersion objective (N.A. 1.4) and 405, 488, and 561 nm laser lines. For each field of view, a stack of two channels (one per staining) and four Z stacks with a step size of 1 µm were acquired. The number of neurons containing one or more red spots versus total cells was determined, and Student's *t*-test was used to compare the values (red dots/cell). The percentage of cells expressing at least one red dot is indicated, along with their S.E.M., at the top of each bar of the graphs. Images of neurons were taken under bright-field microscopy to observe the proper morphology of the cells.

Cellprofiller® pipeline design

First, the ***ColorToGray*** module was used to convert the color images to grayscale for individual channels, Hoechst (blue), PLA dots (red) and NeuN or MAP2 stain (green). This was followed by the application of a ***GaussianFilter*** to smooth the images and reduce noise. Threshold module was employed to segment the NeuN or MAP2 (green) channel and PLA dots (red) channel images, distinguishing the signal from the background. The ***IdentifyPrimaryObjects*** module was used to identify primary objects in the NeuN or MAP2 (green) channel, representing the neuronal structures. Subsequently, the ***IdentifySecondaryObjects*** module was applied to identify secondary objects in the PLA (red) channel, using the primary NeuN or MAP2 objects as a reference.

The ***ShrinkToObjectCenters*** module was then applied to refine the positions by shrinking the objects to their centers, followed by the ***ExpandOrShrinkObjects*** module to adjust the size of the objects if needed to improve accuracy. The ***OverlayOutlines*** module was used to overlay the outlines of identified objects on the original images. Finally, the ***SaveImages*** module was used to save the processed images, and the ***ExportToSpreadsheet*** module was utilized to export the data for further analysis.

Data handling and statistical analysis

GraphPad Prism 10 software (San Diego, CA, USA) was used for data analysis. One-way ANOVA followed by post-hoc Bonferroni's test, post-hoc Tukey's test or Dunnett's test were used when multiple comparison analysis. BRET parameters were calculated using an ad hoc online tool[86]. In PLA assays the number of red dots per cell was determined using with a pipeline specifically designed for the Cellprofiller® software. Two-tailed Student's *t*-test was used for PLA statistical analysis. Statistical analysis was undertaken only when each group size was at least $n = 5$, n being the number of independent variables (technical replicates were not treated as independent variables). Differences were considered significant when $P \leq 0.05$.

Data availability

The data supporting the conclusions of this article are included within the article and its Supplementary file. Additionally, the raw data supporting this article's findings are available from the corresponding author upon request.

Received: 10 April 2024; Accepted: 23 October 2024;
Published online: 15 November 2024

References

1. Hornykiewicz, O. The discovery of dopamine deficiency in the parkinsonian brain. *J. Neural Transm. Suppl.* **70**, 9–15 (2006).
2. Alexander, S. P. et al. The concise guide to pharmacology 2019/20: G protein-coupled receptors. *Br. J. Pharmacol.* **176**, S21–S141 (2019).
3. Hemmings, H., Greengard, P., Tung, H. & Cohen, P. DARPP-32, a dopamine-regulated neuronal phosphoprotein, is a potent inhibitor of protein phosphatase-1. *Nature* **310**, 503–505 (1984).
4. Hemmings, H., Williams, K., Konigsberg, W. & Greengard, P. DARPP-32, a dopamine- and adenosine 3′:5′-monophosphate-regulated neuronal phosphoprotein. I. Amino acid sequence around the phosphorylated threonine. *J. Biol. Chem.* **259**, 14486–14490 (1984).
5. Girault, J. A. & Nairn, A. C. DARPP-32 40 years later. *Adv. Pharmacol.* **90**, 67–87 (2021).
6. Mackie, K. Distribution of Cannabinoid Receptors in the Central and Peripheral Nervous System. in Cannabinoids. *Handbook of*

Experimental Pharmacology, Vol 168 (ed Pertwee, R. G.) 299–325 (Springer, Berlin, Heidelberg, 2005).
7. Han, Q. W., Yuan, Y. H. & Chen, N. H. The therapeutic role of cannabinoid receptors and its agonists or antagonists in Parkinson's disease. *Prog. Neuro-Psychopharmacol. Biol. Psychiatry* **96**, 109745 (2020).
8. Rodríguez-Carreiro, S., Navarro, E., Muñoz, E. & Fernández-Ruiz, J. The cannabigerol derivative VCE-003.2 exerts therapeutic effects in 6-hydroxydopamine-lesioned mice: comparison with the classic dopaminergic replacement therapy. *Brain Sci.* **13**, 1272 (2023).
9. García, C., Palomo-Garo, C., Gómez-Gálvez, Y. & Fernández-Ruiz, J. Cannabinoid–dopamine interactions in the physiology and physiopathology of the basal ganglia. *Br. J. Pharmacol.* **173**, 2069–2079 (2016).
10. de Lago, E. & Fernández-Ruiz, J. Cannabinoids and neuroprotection in motor-related disorders. *CNS Neurol. Disord. Drug Targets* **6**, 377–387 (2007).
11. Kennedy, M. B. Regulation of neuronal function by calcium. *Trends Neurosci.* **12**, 417–420 (1989).
12. Lee, S. P. et al. Dopamine D1 and D2 receptor co-activation generates a novel phospholipase C-mediated calcium signal. *J. Biol. Chem.* **279**, 35671–35678 (2004).
13. Rico, A. J. et al. Neurochemical evidence supporting dopamine D1–D2 receptor heteromers in the striatum of the long-tailed macaque: changes following dopaminergic manipulation. *Brain Struct. Funct.* **222**, 1–18 (2016).
14. Perreault, M. L. et al. The dopamine D1-D2 receptor heteromer localizes in dynorphin/enkephalin neurons: increased high affinity state following amphetamine and in schizophrenia. *J. Biol. Chem.* **285**, 36625–36634 (2010).
15. Rashid, A. J. et al. D1-D2 dopamine receptor heterooligomers with unique pharmacology are coupled to rapid activation of Gq/11 in the striatum. *Proc. Natl Acad. Sci. USA* **104**, 654–659 (2007).
16. Hasbi, A. et al. Dopamine D1-D2 receptor heteromer expression in key brain regions of rat and higher species: upregulation in rat striatum after cocaine administration. *Neurobiol. Dis.* **143**, 105017 (2020).
17. Hasbi, A. et al. A peptide targeting an interaction interface disrupts the dopamine D1-D2 receptor heteromer to block signaling and function in vitro and in vivo: effective selective antagonism. *FASEB J.* **28**, 4806–4820 (2014).
18. Perreault, M. L. et al. Disruption of a dopamine receptor complex amplifies the actions of cocaine. *Eur. Neuropsychopharmacol.* **26**, 1366–1377 (2016).
19. Perreault, M. L., Shen, M. Y. F., Fan, T. & George, S. R. Regulation of c-fos expression by the dopamine D1-D2 receptor heteromer. *Neuroscience* **285**, 194–203 (2015).
20. Verma, V. et al. Dopamine D1-D2 receptor Heteromer-mediated calcium release is desensitized by D1 receptor occupancy with or without signal activation: dual functional regulation by G protein-coupled receptor kinase 2. *J. Biol. Chem.* **285**, 35092–35103 (2010).
21. Hasbi, A. et al. Calcium signaling cascade links dopamine D1-D2 receptor heteromer to striatal BDNF production and neuronal growth. *Proc. Natl Acad. Sci. USA* **106**, 21377–21382 (2009).
22. Picconi, B. et al. Abnormal Ca2+-calmodulin-dependent protein kinase II function mediates synaptic and motor deficits in experimental parkinsonism. *J. Neurosci.* **24**, 5283–5291 (2004).
23. Ibrahim, M. M. RAS inhibition in hypertension. *J. Hum. Hypertens.* **20**, 101–108 (2006). *2006 202*.
24. Labandeira-Garcia, J. L., Valenzuela, R., Costa-Besada, M. A., Villar-Cheda, B. & Rodriguez-Perez, A. I. The intracellular renin–angiotensin system: friend or foe. Some light from the dopaminergic neurons. *Prog. Neurobiol.* **199**, 101919 (2021).
25. Lage, L., Rodriguez-Perez, A. I., Villar-Cheda, B., Labandeira-Garcia, J. L. & Dominguez-Meijide, A. Angiotensin type 1 receptor activation promotes neuronal and glial alpha-synuclein aggregation and transmission. *NPJ Parkinsons Dis.* **10**, 37 (2024).
26. Labandeira-Garcia, J. L. et al. Dopamine-angiotensin interactions in the basal ganglia and their relevance for Parkinson's disease. *Mov. Disord.* **28**, 1337–1342 (2013).
27. Rivas-Santisteban, R. et al. Angiotensin AT1 and AT2 receptor heteromer expression in the hemilesioned rat model of Parkinson's disease that increases with levodopa-induced dyskinesia. *J. Neuroinflammation* **17**, 243 (2020).
28. Villar-Cheda, B. et al. Aging-related dysregulation of dopamine and angiotensin receptor interaction. *Neurobiol. Aging* **35**, 1726–1738 (2014).
29. Occhieppo, V., Basmadjian, O. & Bregonzio, C. Brain angiotensin II in dopaminergic imbalance-derived pathologies: Neuroinflammation and vascular responses. *Neural Regen. Res.* **16**, 504–505 (2021).
30. Labandeira, C. M. et al. Angiotensin type-1 receptor and ACE2 autoantibodies in Parkinson´s disease. *NPJ Parkinsons Dis.* **8**, 1–12 (2022). *2022 81*.
31. Martirosyan, A. et al. Unravelling cell type-specific responses to Parkinson's Disease at single cell resolution. *Mol. Neurodegener.* **19**, 1–24 (2024).
32. Lee, A. J. et al. Characterization of altered molecular mechanisms in Parkinson's disease through cell type-resolved multiomics analyses. *Sci. Adv.* **9**, eabo2467 (2023).
33. Kamath, T. et al. Single-cell genomic profiling of human dopamine neurons identifies a population that selectively degenerates in Parkinson's disease. *Nat. Neurosci.* **25**, 588–595 (2022).
34. Rozenfeld, R. et al. AT_1R-CB_1R heteromerization reveals a new mechanism for the pathogenic properties of angiotensin II. *EMBO J.* **30**, 2350–2363 (2011).
35. Lopez, A. & Munoz, J. Mechanisms of the effects of exogenous levodopa on the dopamine-denervated striatum. *Neuroscience* **103**, 639–651 (2001).
36. Muñoz, A. et al. Combined 5-HT1A and 5-HT1B receptor agonists for the treatment of l-DOPA-induced dyskinesia. *Brain* **131**, 3380–3394 (2008).
37. Fernández-Ruiz, J., Moro, M. A. & Martínez-Orgado, J. Cannabinoids in neurodegenerative disorders and stroke/brain trauma: from preclinical models to clinical applications. *Neurotherapeutics* **12**, 793–806 (2015).
38. Campbell, V. A. & Gowran, A. Alzheimer's disease; taking the edge off with cannabinoids? *Br. J. Pharmacol.* **152**, 655–662 (2009).
39. Rodríguez-Cueto, C. et al. Neuroprotective effects of the cannabigerol quinone derivative VCE-003.2 in SOD1G93A transgenic mice, an experimental model of amyotrophic lateral sclerosis. *Biochem. Pharmacol.* **157**, 217–226 (2018).
40. Sagredo, O. et al. Cannabinoid CB2 receptor agonists protect the striatum against malonate toxicity: relevance for Huntington's disease. *Glia* **57**, 1154–1167 (2009).
41. Solimini, R., Rotolo, M. C., Pichini, S. & Pacifici, R. Neurological disorders in medical use of cannabis: an update. *CNS Neurol. Disord. Drug Targets* **16**, 527–533 (2017).
42. de Barros Viana, M., de Aquino, P. E. A., Estadella, D., Ribeiro, D. A. & de Barros Viana, G. S. *Cannabis sativa* and cannabidiol: a therapeutic strategy for the treatment of neurodegenerative diseases? *Med. Cannabis Cannabinoids* **5**, 207–219 (2022).
43. Pascual, A. C., Gaveglio, V. L., Giusto, N. M. & Pasquaré, S. J. 2-Arachidonoylglycerol metabolism is differently modulated by oligomeric and fibrillar conformations of amyloid beta in synaptic terminals. *Neuroscience* **362**, 168–180 (2017).
44. Pérez-Olives, C., Rivas-Santisteban, R., Lillo, J., Navarro, G. & Franco, R. Recent advances in the potential of cannabinoids for neuroprotection in Alzheimer's, Parkinson's, and Huntington's diseases. in *Advances in Experimental Medicine and Biology,* Vol. 1264, 81–92 (Springer, 2021).

45. Aso, E. & Ferrer, I. Cannabinoids for treatment of Alzheimer's disease: moving toward the clinic. *Front. Pharmacol.* **5**, 37 (2014).
46. Aymerich, M. S. et al. Cannabinoid pharmacology/therapeutics in chronic degenerative disorders affecting the central nervous system. *Biochem. Pharmacol.* **157**, 67–84 (2018).
47. Ferré, S. et al. Calcium-mediated modulation of the quaternary structure and function of adenosine A2A-dopamine D2 receptor heteromers. *Curr. Opin. Pharmacol.* **10**, 67–72 (2010).
48. Navarro, G. et al. Interactions between calmodulin, adenosine A2A, and dopamine D2 receptors. *J. Biol. Chem.* **284**, 28058–28068 (2009).
49. O'Day, D. H. The complex interplay between toxic hallmark proteins, calmodulin-binding proteins, ion channels, and receptors involved in calcium dyshomeostasis in neurodegeneration. *Biomolecules* **14**, 173 (2024).
50. Franco, N. & Franco, R. Understanding the added value of G-protein-coupled receptor heteromers. *Scientifica* **2014**, 362937 (2014).
51. Franco, R. & Navarro, G. Neuroprotection afforded by targeting G protein-coupled receptors in heteromers and by heteromer-selective drugs. *Front. Pharmacol.* **14**, 1222158 (2023).
52. Casadó, V. et al. GPCR homomers and heteromers: a better choice as targets for drug development than GPCR monomers? *Pharmacol. Ther.* **124**, 248–257 (2009).
53. Martínez-Pinilla, E. et al. Dopamine D2 and angiotensin II type 1 receptors form functional heteromers in rat striatum. *Biochem. Pharmacol.* **96**, 131–142 (2015).
54. Kobiec, T. et al. The renin–angiotensin system modulates dopaminergic neurotransmission: a new player on the scene. *Front. Synaptic Neurosci.* **13**, 8519 (2021).
55. Ferré, S., Goldberg, S. R., Lluis, C. & Franco, R. Looking for the role of cannabinoid receptor heteromers in striatal function. *Neuropharmacology* **56**, 226–234 (2009).
56. Franco, R. et al. G-protein-coupled receptor heteromers: function and ligand pharmacology. *Br. J. Pharmacol.* **153**, S90–S98 (2008).
57. Kenakin, T., Watson, C., Muniz-Medina, V., Christopoulos, A. & Novick, S. A simple method for quantifying functional selectivity and agonist bias. *ACS Chem. Neurosci.* **3**, 193–203 (2012).
58. Kenakin, T. Biased agonism. *F1000 Biol. Rep.* **1**, 87 (2009).
59. Khajehali, E. et al. Biased agonism and biased allosteric modulation at the CB1 cannabinoid receptors. *Mol. Pharmacol.* **88**, 368–379 (2015).
60. Urban, J. D. et al. Functional selectivity and classical concepts of quantitative pharmacology. *J. Pharmacol. Exp. Ther.* **320**, 1–13 (2007).
61. Sierra, S. et al. Detection of cannabinoid receptors CB1 and CB2 within basal ganglia output neurons in macaques: changes following experimental parkinsonism. *Brain Struct. Funct.* **220**, 2721–2738 (2015).
62. Pinna, A. et al. L-DOPA disrupts adenosine A_{2A}-cannabinoid CB_1-dopamine D_2 receptor heteromer cross-talk in the striatum of hemiparkinsonian rats: biochemical and behavioral studies. *Exp. Neurol.* **253**, 180–191 (2014).
63. Bonaventura, J. et al. L-DOPA-treatment in primates disrupts the expression of A_{2A} adenosine-CB_1 cannabinoid-D_2 dopamine receptor heteromers in the caudate nucleus. *Neuropharmacology* **79**, 90–100 (2014).
64. Martínez-Pinilla, E. et al. Expression of GPR55 and either cannabinoid CB_1 or CB_2 heteroreceptor complexes in the caudate, putamen, and accumbens nuclei of control, parkinsonian, and dyskinetic non-human primates. *Brain Struct. Funct.* **225**, 2153–2164 (2020).
65. Martínez-Pinilla, E. et al. CB1 and GPR55 receptors are co-expressed and form heteromers in rat and monkey striatum. *Exp. Neurol.* **261**, 44–52 (2014).
66. Muñoz, A., Garrido-Gil, P., Dominguez-Meijide, A. & Labandeira-Garcia, J. L. Angiotensin type 1 receptor blockage reduces L-dopa-induced dyskinesia in the 6-OHDA model of Parkinson's disease. Involvement of vascular endothelial growth factor and interleukin-1ß. *Exp. Neurol.* **261**, 720–732 (2014).
67. Booth, H. D. E., Hirst, W. D. & Wade-Martins, R. The role of astrocyte dysfunction in Parkinson's disease pathogenesis. *Trends Neurosci.* **40**, 358 (2017).
68. Chavarría, C., Ivagnes, R. & Souza, J. M. Extracellular alpha-synuclein: mechanisms for glial cell internalization and activation. *Biomolecules* **12**, 655 (2022).
69. Valenzuela, R. et al. Mitochondrial angiotensin receptors in dopaminergic neurons. Role in cell protection and aging-related vulnerability to neurodegeneration. *Cell Death Dis.* **7**, e2427 (2016).
70. Bénard, G. et al. Mitochondrial CB_1 receptors regulate neuronal energy metabolism. *Nat. Neurosci.* **15**, 558–564 (2012).
71. Ashrafi, G., Schlehe, J. S., LaVoie, M. J. & Schwarz, T. L. Mitophagy of damaged mitochondria occurs locally in distal neuronal axons and requires PINK1 and Parkin. *J. Cell Biol.* **206**, 655–670 (2014).
72. Park, J. et al. Mitochondrial dysfunction in *Drosophila* PINK1 mutants is complemented by parkin. *Nature* **441**, 1157–1161 (2006).
73. Goyal, S. & Chaturvedi, R. K. Mitochondrial protein import dysfunction in pathogenesis of neurodegenerative diseases. *Mol. Neurobiol.* https://doi.org/10.1007/s12035-020-02200-0 (2020).
74. Vila, M., Ramonet, D. & Perier, C. Mitochondrial alterations in Parkinson's disease: new clues. *J. Neurochem.* **107**, 317–328 (2008).
75. Franco, R., Rivas-Santisteban, R., Navarro, G., Pinna, A. & Reyes-Resina, I. Genes implicated in familial Parkinson's disease provide a dual picture of nigral dopaminergic neurodegeneration with mitochondria taking center stage. *Int. J. Mol. Sci.* **22**, 4643 (2021).
76. Lillo, A. et al. Targeted metabolomics shows that the level of glutamine, kynurenine, acyl-carnitines and lysophosphatidylcholines is significantly increased in the aqueous humor of glaucoma patients. *Front. Med.* **9**, 2082 (2022).
77. Franco, R. & Serrano-Marín, J. The unbroken Krebs cycle. Hormonal-like regulation and mitochondrial signaling to control mitophagy and prevent cell death. *BioEssays* https://doi.org/10.1002/BIES.202200194 (2022).
78. Hradsky, J., Mikhaylova, M., Karpova, A., Kreutz, M. R. & Zuschratter, W. Super-resolution microscopy of the neuronal calcium-binding proteins Calneuron-1 and Caldendrin. *Methods Mol. Biol.* **963**, 147–169 (2013).
79. Franco, R. et al. *N*-Methyl-D-aspartate receptor link to the MAP kinase pathway in cortical and hippocampal neurons and microglia is dependent on calcium sensors and is blocked by α-Synuclein, Tau, and Phospho-Tau in non-transgenic and transgenic $APP_{Sw,Ind}$ mice. *Front. Mol. Neurosci.* **11**, 273 (2018).
80. Lopez-Lopez, A. et al. Interactions between angiotensin type-1 antagonists, statins, and ROCK inhibitors in a rat model of L-DOPA-induced dyskinesia. *Antioxidants* **12**, 1454 (2023).
81. Lopez-Lopez, A., Labandeira, C. M., Labandeira-Garcia, J. L. & Muñoz, A. Rho kinase inhibitor fasudil reduces L-DOPA-induced dyskinesia in a rat model of Parkinson's disease. *Br. J. Pharmacol.* **177**, 5622–5641 (2020).
82. Winkler, C., Kirik, D., Björklund, A. & Cenci, M. A. L-DOPA-induced dyskinesia in the intrastriatal 6-hydroxydopamine model of Parkinson's disease: relation to motor and cellular parameters of nigrostriatal function. *Neurobiol. Dis.* **10**, 165–186 (2002).
83. Kirik, D., Winkler, C. & Björklund, A. Growth and functional efficacy of intrastriatal nigral transplants depend on the extent of nigrostriatal degeneration. *J. Neurosci.* **21**, 2889–2896 (2001).
84. Farré, D. et al. Stronger dopamine D1 receptor-mediated neurotransmission in dyskinesia. *Mol. Neurobiol.* **52**, 1408–1420 (2015).
85. Chen, T.-W. et al. Ultrasensitive fluorescent proteins for imaging neuronal activity. *Nature* **499**, 295–300 (2013).
86. Herraez, A. BRET analysis. https://biomodel.uah.es/lab/calculos/regresion/BRET.htm (2022).

Acknowledgements
The University of Barcelona's laboratories are considered excellent research groups (grup consolidat #2021 SGR 00304) by the Regional Catalonian Government. This work was supported by grants and PID 2020-113430RB-I00 (to G.N.) PID2021-126600OB-I00 (to R.F.) funded by Spanish MCIN/AEI/10.13039/501100011033 and, as appropriate, by "ERDF A way of making Europe", by the "European Union" or by the "European Union Next Generation EU/PRTR".

Author contributions
R.F., J.L.L.G., and G.N. participated in conceptualization and experimental design. R.R.S. did BRET, PLA, cAMP, and ERK phosphorylation assays. R.R.S. and J.L. participated in assays of determination of cytoplasmic calcium levels. A.M. and A.I.R.P. prepared lesioned animals and obtained the brain samples. R.R.S., I.R., and J.L. participated in the preparation of primary cultures. R.R.S. prepared figures. R.F. wrote the first draft. R.F., J.L.L.G., R.R.S., J.L., A.M., A.I.R.P., and G.N. edited the article. All authors approved the submitted version.

Competing interests
The authors declare no competing interests.

Ethical approval
Animal handling, sacrifice, and further experiments were conducted according to the guidelines set in Directive 2010/63/EU of the European Parliament and the Council of the European Union that are enforced in Spain by National and Regional organisms; the 3R rule (replace, refine, reduce) for animal experimentation was also considered. The rat PD model was generated and handled using a protocol approved by the Ethical Committee of the University of Santiago de Compostela (Protocol 14715012/2021/012; last revision 16 April 2021). According to the current legislation, protocol approval is unnecessary if animals are sacrificed to obtain a specific tissue as in this work to obtain primary neurons.

Additional information
Supplementary information The online version contains supplementary material available at https://doi.org/10.1038/s41531-024-00827-7.

Correspondence and requests for materials should be addressed to Rafael Rivas-Santisteban or Rafael Franco.

Reprints and permissions information is available at http://www.nature.com/reprints

Publisher's note Springer Nature remains neutral with regard to jurisdictional claims in published maps and institutional affiliations.

Open Access This article is licensed under a Creative Commons Attribution-NonCommercial-NoDerivatives 4.0 International License, which permits any non-commercial use, sharing, distribution and reproduction in any medium or format, as long as you give appropriate credit to the original author(s) and the source, provide a link to the Creative Commons licence, and indicate if you modified the licensed material. You do not have permission under this licence to share adapted material derived from this article or parts of it. The images or other third party material in this article are included in the article's Creative Commons licence, unless indicated otherwise in a credit line to the material. If material is not included in the article's Creative Commons licence and your intended use is not permitted by statutory regulation or exceeds the permitted use, you will need to obtain permission directly from the copyright holder. To view a copy of this licence, visit http://creativecommons.org/licenses/by-nc-nd/4.0/.

© The Author(s) 2024